NASA TT-F-11,421

NASA TT-F-11,421

EFFECT OF CURVED SURFACES ON TURBULENT BOUNDARY LAYERS

H. Wilcken

Translation of "Turbulente Grenzschichten an gewoelbten Flaechen."
Berlin, Vol 1, No 4, Sept 1930, pp 357-376

NATIONAL AERONAUTICS AND SPACE ADMINISTRATION
WASHINGTON
DEC 1967

EFFECT OF CURVED SURFACES ON TURBULENT BOUNDARY LAYERS[1]

H. Wilcken

Introduction

When a liquid flows along a wall the layer of the liquid next to the wall is slowed down due to the friction and forms a so-called boundary or friction layer, in which the speed next to the wall gradually is reduced to the value of zero. In most practical cases the flow in this boundary layer is not laminar but turbulent. Since, as Prandtl[2] has demonstrated, this boundary layer is the key to understanding energy losses and resistance in flow movement, thorough research into the phenomena connected with these turbulent boundary layers is of extraordinary importance. For straight, smooth walls without significant loss of pressure along the line of flow the most important laws concerning this boundary layer flow, in particular the speed distribution, have to some degree been explored[3]. Work has also been done on the influence of a pressure drop (pressure reduction and pressure increase)[4] and of wall unevenness[5]. It was also assumed that a curve in the wall in the direction of the flow influences the boundary layer phenomena. That is, because the various parts of the boundary layer are variously affected by centrifugal force in the presence of a curved surface, a concave surface produces a tendency to force the fast parts of the flow toward the surface and the slow parts away from it. This tendency favors the exchange of the slow layers next to the surface with the faster ones on the inside of the flow. Thus it reinforces the already existing turbulent exchange procedure. The contrary is the case for convex surfaces. Here the centrifugal force has a stabilizing effect, reducing the turbulence. About the degree of this influence, however, nothing was known up to the present time.

The investigation described in the following was undertaken for the purpose clarifying this influence of curvature upon turbulent boundary layers[6]. The inner and outer walls of a curve of rectangular cross section served as the curved surfaces. A number of investigations on flow phenomena against curvatures have already been undertaken in the abstract[7]. However, these concern a significantly different phenomenon, namely the so-called secondary flows. Because the fast parts of a flow are forced outward, two secondary flows arise, which superimpose themselves helically upon the main flow.

As explained above, however, the problem examined in the present work is a significantly different one. Here, the experimental equipment must be so arranged that the secondary flows are as small as possible because observation of the phenomena connected with the problem is considerably more difficult. This was accomplished by making the dimension of the curved surface cross section considerable shorter in the radial direction than in height, so that quite good flow conditions were obtained, except for the upper and lower portions of the curved surface. Measurements at various heights on the curved surface confirmed this assumption.

The experiments were carried out with air. Compared to water, this has the advantage that adequately large dimensions of the experimental objects can relatively easily be used, and that the measurements are more easily taken. The speeds used did not exceed 25 m/sec, so that the air was to be dealt with as an inelastic flow, since air compressibility makes itself felt only in the neighborhood of the speed of sound.

I. Experiments

1. Experiment Apparatus

The walls of the curved chamber in which the experiments were carried out were of sheet brass, one millimeter thick; the cover and bottom were made of wood. The experiment apparatus used for the main experiments is shown in Fig. 1. The air is sucked into the chamber by the fan, G. It enters through a straightener, G1, is led through a suitable entrance duct to the curved chamber, where it is deflected 180 degrees. From the chamber an expanded duct leads to the fan. The cross section of the curved channel was rectangular, height was 65 centimeters, the vertical distance

between the walls 9.5 cm, and curve radii of the walls 40.5 and 50 cm, respectively. Iron rings, p, were screwed to the chamber walls for reinforcement. Wooden rings, o, of square cross section were fastened to the reinforcement, into which splines were set next to the brass walls of the chamber. Square rubber strips made the splines air-tight. The entire curved chamber apparatus was firmly screwed to the bottom, m. the cover was fastened to the chamber with clamps in order to facilitate its removal and replacement. The straightener at the air intake was composed of strips of sheet zinc criss-crossed to form tubes 15 cm long and 5 x 5 cm in cross section. The exhaust fan was a four-bladed ventilator, attached to the axle of the motor, m. A rheostat connected to the motor permitted regulation of the motor revolutions and thereby the amount of the air flow.

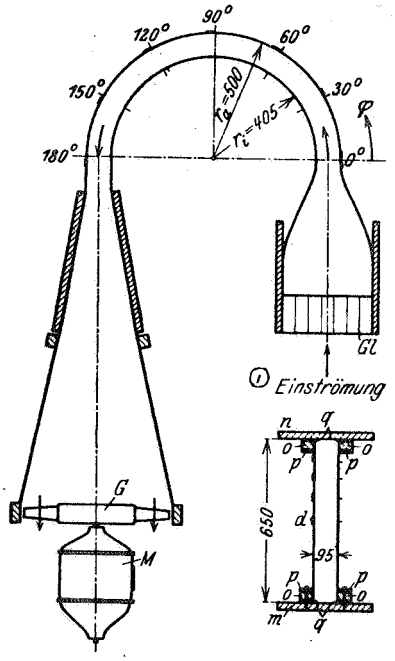

Fig. 1. Experimental Apparatus for Slight Curvature

[Legend]: 1) Air inflow.

Prior to the main experiments with the apparatus just described, a number of other devices were tried out, which however, proved less suitable for the intended purposes. One

of these is shown in Fig. 2. (Curve radii 10 cm and 20 cm or 15 and 20 cm.) In addition, an entrance channel, consisting of parallel walls of wood, is found between the straightener box and the beginning of the curvature channel.

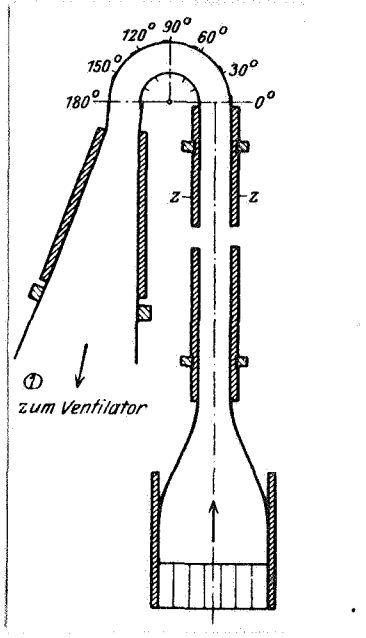

Fig. 2. Experiment Device for Strong Curvature

[Legend]: 1) To fan.

In the experiments the static pressure on the chamber walls was taken by means of fine drill holes, .4 mm in diameter, in the middle horizontal section. The pressure measurement points were for the inner and outer walls separated by 30°, with the starting point at 0° (shown by dashes in Figs 1 and 2.) Within the chamber the static pressure was measured by means of a simple probe, provided, at a distance of two centimeters from the streamlined inlet, with six fine drill holes. The overall pressure was measured with a Pitot tube, made from a fine steel tube of .4 mm outside diameter and .3 mm inside diameter and placed on a streamlined supply line. For close approach to the wall, the steel tube was bent in an S-shape toward the wall (different for the inner and outer walls.) The pressure measuring device was introduced through the outer wall, drilled for the purpose at the measuring points. By means of a micrometer screw which could

be screwed onto a flange soldered to the wall, the measuring device could be pushed through the chamber. Fig. 3 shows a measuring point with micrometer screw and Pitot tube.

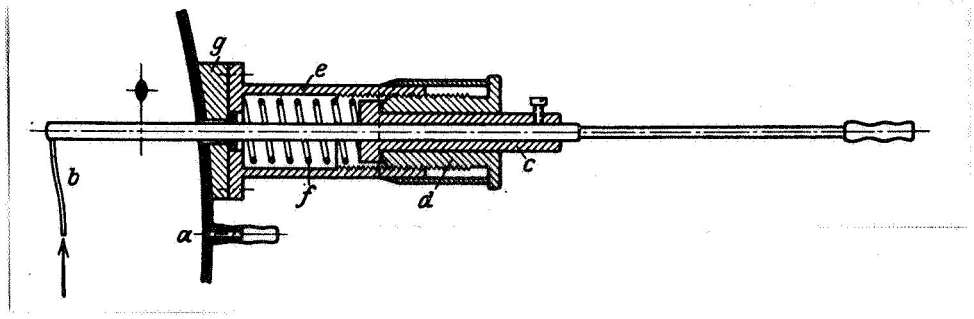

Fig. 3. Pressure measuring connection on the chamber wall (a) and pitot tube (b) with operating mechanism (pitot tube Holder, c; Threaded Spindle, d; Casing, e; Spring, f; base, g.)

For measuring static and overall pressure micromanometers with obliquely placed measuring tubes were used, and for control of the amount of flow a manometer of Prandtl's design.

Figs 4 and 5 show the entire experimental installation. Fig 4 shows in the foreground the straightener and the motor with the fan, Fig 5 the other side, with the arrangement of the measuring points and the fastening of the cover by means of clamps.

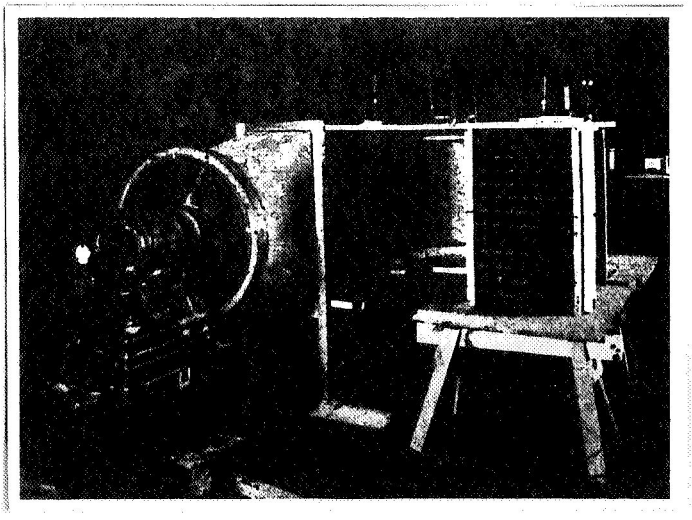

Fig. 4. Experimental installation, intake and fan

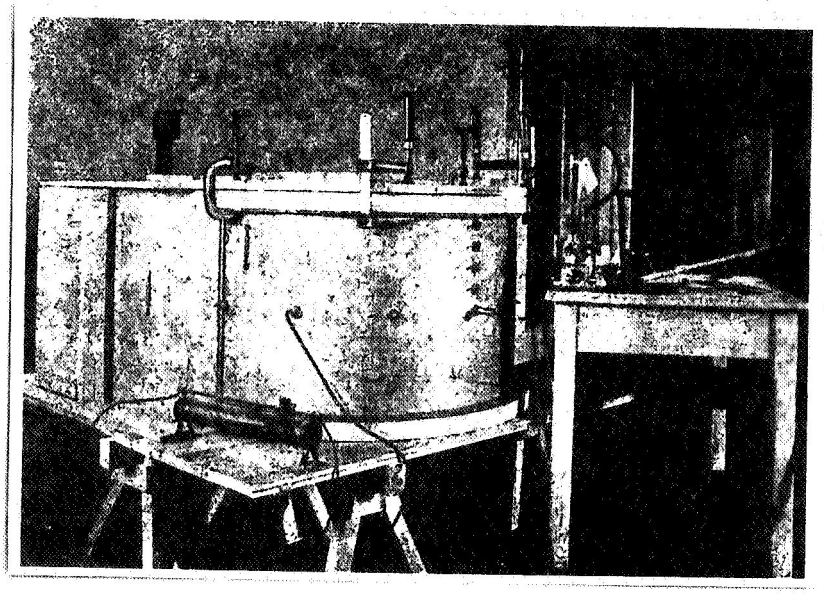

Fig. 5. Experimental installation, the curved chamber and measuring points

2. The Measuring

As already mentioned, the chamber walls were high in relation to the distance between them so that an even flow might be obtained in the middle section of the channel. For determination of the limits within which this held true additional measuring points were placed 90° on the vertical so that measurements could be taken to within 7 cm of the lid. The speed profile found at these points is shown in Fig. 6. The effect of the lid or the bottom is to be reckoned with at a distance approximately equal to the width of the channel, i.e., approximately 10 cm from the lid. In the evaluations, therefore, it was permissible with good approximation to regard the layer extending from 10 cm below the lid to 10 above the bottom as an even flow.

In all, three different chambers were investigated, in part with, in part without approach channels, so that seven different series of experiments resulted:

1) Versuchs-reihe	2) Krümmungsradien in cm		5) Kanalweite in cm	6) Anlaufstrecke in m	7) Einlauf	8) Mittlere Geschwindigkeiten v_m in m/sek		
	3) innen	4) außen						
A	10	20	10	3	9) symmetrisch	11,	12,5,	14
B	15	20	5	3	,,	11,5,		14
C	15	20	5	1	,,	9,2,		13,1
D	10	20	10	1	10) ,,	12,42,	14,36,	15,95
E	10	20	10	0	unsymmetr.	—	—	—
F	10	20	10	0	symmetrisch	11,3,	15,4,	17,2
H	40,5	5°	9,5	0	9) ,,	12,7,	18,4,	19,3

[Legend]: 1) Experiment; 2) Curvature radii in cm; 3) Inner; 4) Outer; 5) Channel width in cm; 6) Approach channel; 7) Intake; 8) Median speeds v_m in m/sec; 9) Symmetrical; 10) Asymmetrical.

In general, each series of experiments was carried out at three different speeds in order that a possible effect of the Reynolds factor $R = v_m a/v$ (v, kinematic viscosity; a, distance between channel walls; v_m, median speed = amount of flow; cross section) might be determined. In the B and C series only two speeds were worked with, because already after the first measurements it was apparent that the results produced nothing new or could not be evaluated. The E series was broken off after a few preliminary measurements. The speed v_m was determined from the pressure drop at the intake.

The first measurements were begun with determination of the overall pressure:

$$G = p + \frac{\varrho v^2}{2}$$

Next, measurements were taken to the middle of the chamber and then from the inner wall to the middle. The micrometer position in which the Pitot tube touches the wall, i.e., the initial point for measuring the distance of the tube from the wall, is easily determined in the following manner. The Pitot tube is turned in so close to the wall that its point lies against the wall and the small tube is somewhat elastically bent. If the tube is then inserted farther into the chamber, with simultaneous measuring of the overall pressure, the overall pressure naturally remains unchanged as long as the tip of the small tube remains in contact with the wall. At the moment when the small tube no longer touches the wall, a rapid change in pressure is observed, since in the vicinity of the wall there is a strong drop in the pressure. In this

way the zero position could be determined with an exactitude of .1 mm. Since the tip of the Pitot tube had an outside diameter of .4 mm, the first measuring point was established at .2 mm from the wall. The holes for insertion of the Pitot tube must, to the extent they are not used directly, be carefully sealed and smoothed with plasticine.

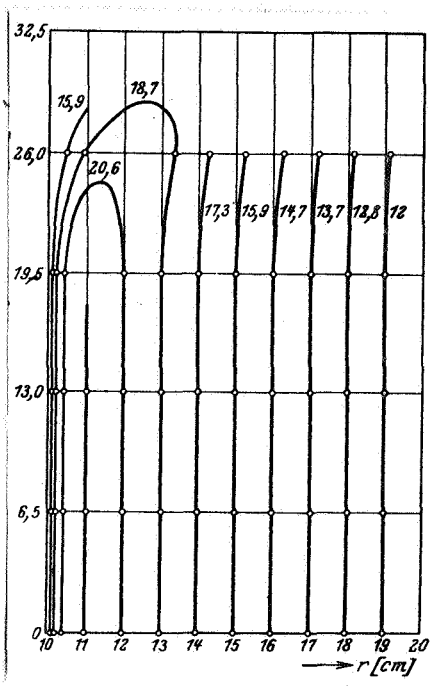

Fig. 6. Lines of equal speed in cross section. $\varphi = 90°$. Experiment series D, v_m = 15.95 m/sec.

For determination of the overall pressure, 23 measuring points were established over the cross section. A third fixed Pitot tube was inserted into the straightener box through the cover. This Pitot tube gives the overall pressure of the potential flow, since according to Bernoulli's equation the potential flow remains constant in the entire area. This Pitot tube served as the zero point for the other pressures, in that the potential flow was measured with a manometer with respect to its difference with this overall pressure. The pressure outside the curved chamber could not be used as the zero point because a small energy loss was caused by the straightener, so that the outside pressure was always somewhere higher than the overall pressure of the potential flow.

For determination of static pressures, nine points were selected over the cross section for a given median speed, so that eleven points had to be measured out on the wall at intervals of 10 mm. Between individual readings the control micromanometer was constantly checked and the pressure drop in the chamber entrance, which had to be kept constant, adjusted when fluctuations in the speed of the fan motor occurred. Prior to the beginning of an experiment series the manometer was cakibrated, establishing the calibration factor for the entire series. Next, everything was tested for leaks. Barometric pressure and temperature readings were taken before and after the determination of a cross section profile and their average arithmetical value used, perhaps after some adjustment.

3. Correction of the Measured Statical Pressures

In measuring the static pressure by means of a direct, laterally inserted probe, a prerequisite for obtaining correct results is that the flow lines are straight and run parallel to the probe, i.s., that the flow is symmetrical around the probe. In the curved chamber the flow lines are curved and in addition radial speed components are present, especially in its first part; thus the flow is not symmetrical around the probe. The greatest disturbances occur in the vicinity of the outer and inner walls because here the probe readings are considerably influenced by the adjacent walls; the deviation here, however, amounted to no more than 10 percent. An attempt was therefore made to compensate for the errors by mathematical means.

For correction of the measured static pressures the circumstance was utilized that the differential coefficient of the static pressure at a certain point depends on the radius of the centrifugal force of the curved flow. Owing to the radial velocity components one more term must be introduced, namely $\varrho v\, dw/rd\varphi$. Thus we write

$$\frac{dp}{dr} = \frac{\varrho v^2}{r} - \varrho v \frac{dw}{r d\varphi}, \qquad (1)$$

where p is the static pressure, v the speed, w the radial speed, r the radius, and ϱ the density of the medium. The term $-\varrho v\, dw/rd$ can generally be ignored, since only in experiments with strong curvature in the measuring cross sections 0° and 30° does it amount to about 5% of the term $\varrho v^2/r$. Elsewhere it remains under 1%.

The total pressure is

$$G = p + \frac{\varrho v^2}{2}; \tag{2}$$

thus for each point

$$\varrho v^2 = 2(G - p).$$

This introduced into (1) gives

$$\frac{dp}{dr} = \frac{2}{r}(G - p).$$

When we now introduce the pressure differences against the pressure p_i at the inner wall, we obtain

$$\frac{d(p - p_i)}{dr} = \frac{2}{r}[(G - p_i) - (p - p_i)]. \tag{3}$$

This is a linear differential equation of the first order. The solution, the correctness of which can easily be proven, is

$$p - p_i = \frac{1}{r^2}\int_{r_i}^{r} (G - p_i)\, 2r\, dr. \tag{4}$$

Thus in order to determine the static pressure it is necessary only that the pressure at the inner wall p_i and the distribution of the total pressure G over the cross section be known, and this is established with adequate accuracy by means of the measuring. The static pressure p_a obtained the outer wall serves as a check.

4. Experiments with Strong Curvatures

Since it was not known in advance how great the curvature influences to be investigated were, chambers of relatively short radii (strong curvature, Fig 2) were next investigated in order, if possible, to obtain an effect of the kind to be expected.

The strong curvature, however, had the disadvantage that a matching pressure increase appeared at the outer side. But since during a pressure increase the boundary layer is very greatly broadened, the influence of the wall curvature was very difficult to separate from the influences of the pressure rise. Contrary to expectation, the influence of the curvature proved extraordinarily great.

The first experiments were undertaken in a 180° chamber, with inner radius of 10 cm and outer radius of 20 cm

(Fig. 2). A straight entrance channel 3 m in length, without rounded off surfaces,was placed ahead of the beginning of the curve. According to the Blasius formula, for turbulent boundary layer thickness, no area of potential flow was to be expected in this channel at the beginning of the curvature. A stationary flow condition, as perhaps might be conjectured after a certain angle in the curved chamber, did not show up. In addition, the fluctuations of the manometer were so great during the measuring that the velocities could not be determined with adequate accuracy. For overcoming the main interferences, the straightener was next placed ahead of the entrance channel and a large wire screen ahead of the straightener, so that the great turbulence originating from the fan were to a large extent eliminated before they reached the entrance stretch (experiment Series A.)

In order to obtain separately the effects of concave and convex curvatures, it was desirable to make the arrangements so that the boundary layers on the outer and inner sides of the chamber were separated by a middle layer in which potential flow existed. To provide for this the entrance channel was shortened to one meter (Series D), so that at the beginning of the curvature a boundary layer 2.5 cm thick was present at each side. At the outer wall the measurements now showed a very high pressure rise, stretching from approximately 0° to 60°. A pressure rise always brings with it slower speed and increased turbulence, and to the pressure rise is added the effect of the curvature, so that at the angle of 90° the boundary layers occupy the entire cross section. In the areas free from the disturbing effects andalone came into question for evaluation of the curvature effect, there was no longer an area of potential flow. In order now to make further pursuit of boundary layer development possible, the one-meter-long entrance channel was removed and the straightener box attached directly to the curved chamber, making the boundary layer thickness as small as possible at the beginning. It amounted to only a few millimeters (Experiment Series F.) But since the curvature radii remained the same, the pressure increase p_a at the outer wall and the pressure decrease p_i at the inner wall were still present (Figs 7 and 8.) To be sure, this no longer had so great an effect upon the thickness of the boundary layer, because at the beginning of the curve it was almost zero.

For the purpose of eliminating the disturbing pressure increase at the outer wall and the great pressure drop at the inner wall, as well as observation of the boundary layer development purely under the influence of centrifugal force,

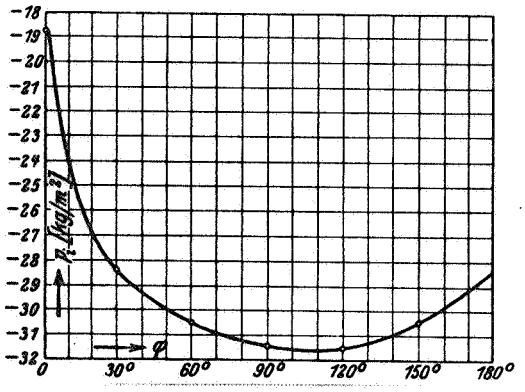

Fig. 7. Pressure at the inner wall in experiment series F (strong curvature) v_m = 15.4 m/sec

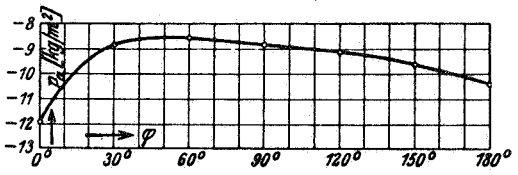

Fig. 8. Pressure at the outer wall in experiment seris F (strong curvature) v_m = 15.4 m/sec

an attempt was made so to shape the entrance channel that already at the entrance to the curved chamber a potential flow would be present, which would to some degree approach the later stationary condition (vr = constant.) Since the velocities in the subsequent flow do not significantly change, the pressure will also to some degree remain constant. To attain this, the cross section of a channel with parallel walls and a symmetrical entrance was pictured, conforming to a function $\varphi = e^z$. In this picture the straight lines of the z planes x = const are transformed into the circles of the φ planes, i.e., the parallel walls of a curved chamber. The symmetrical entrance to the straight channel is transformed into an asymmetrical one at the curved chamber. An entrance corresponding to this picture was now set in front of the curved chamber. The former disturbing effect of the pressure rise was almost eliminated by means of this specially shaped sheet metal, but because of space limitations the installation could not be completely realized, so that nl completely satisfactory potential flow resulted. This experiment series was therefore not completed, only the static

pressures being measured.

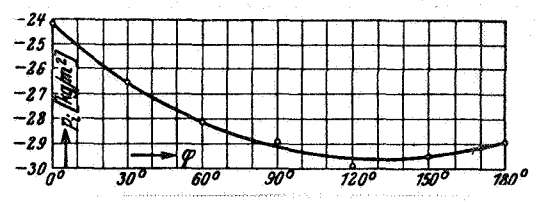

Fig. 9. Pressures at the inner wall in experiment series H (weak curve) v_m = 18.4 m/sec

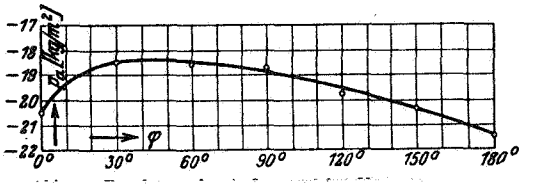

Fig. 10. Pressure at the outer wall in experiment series H (weak curve) v_m = 18.4 m/sec

5. Experiments with Weaker Curvatures

Because the experiments with strong curvatures showed that in every case the influence of the curvature is very great, and because in strong curvature satisfactory separation of the curvature influence from other influences met with considerably difficulty, a new curved chamber was built, with radii of 40.5 and 50 cm, i.e., a chamber of significantly weaker curvatures (Fig. 1.) The weak curvature had the advantage that at the outer wall, from about 0° to 50°, there was only a slight pressure increase (Fig. 9 and 10.) Since in addition no entrance channel was used, the straightener being directly attached to the chamber, the boundary layer at the beginning of the curvature, where the pressure increase becomes effective, was very thin. Therefore the abnormal condition found in the boundary layer could be largely ascribed to the effect of centrifugal force upon the turbulence in the boundary layer. From comparison of the results obtained with this arrangement (Series H) with those obtained with very strong curvature, it can be concluded, however,

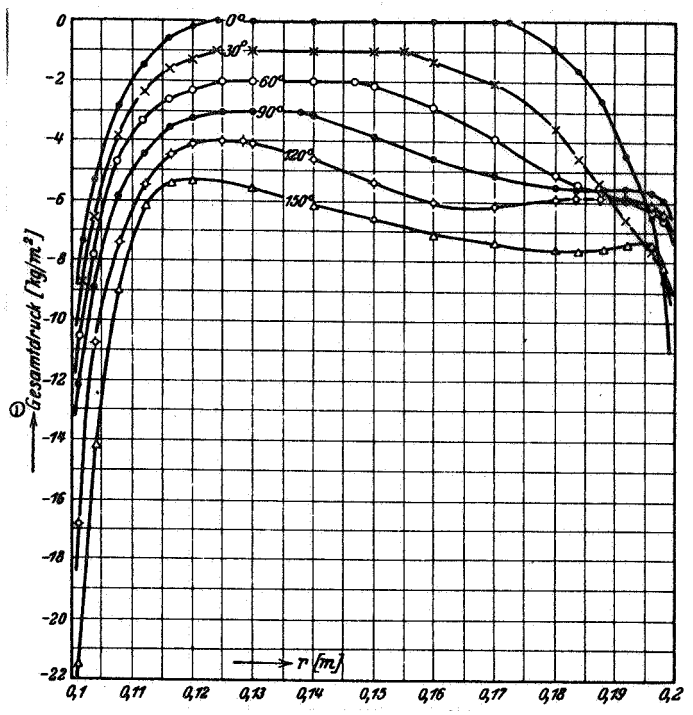

Fig. 11. Total pressures in experiment series D (weak curve, 1 m entrance channel). v_m = 15.95 m/sec. The scale of the pressures refer to $\varphi = 0°$; the curves for the following angles are always displaced lower by 1 kg/m^2.

[Legend]: 1) Total pressure.

that in the latter as well the results apparently depended mainly on centrifugal force and were not significantly affected by the rise in pressure.

6. Review of the Flow Conditions Found

If one observes the total pressures plotted over the radii of the middle horizontal cross section, one sees that with an entrance stretch of one meter some potential flow still remains at the 120° measuring point (Fig. 11.) Boundary layer thickness increases greatly at the outer wall, while at the inner wall it remains almost constant with the increasing angle.

At stronger curvature and larger angles, that is, where no potential flow any longer exists, the total pressure

curves show, with increasing distance from the outer wall, after an initial rise, a striking reduction, followed by another rise to the maximum (see Fig 11, at 120° and 150°.) This was observed to be especially strong in experiment series A. The statis pressure curves arenot shown in Fig 11, because their development offers nothing noteworthy compared to the Figures that follows. The corrected static pressures are shown in Figs 12 and 13. The total pressure profile of experiment series F (Fig 12) presents another picture to the extent that the boundary layer thickness at the inner side of the chamber amounts to only a few millimeters. The fall in the total pressure observed in experiment series A and D after an initial rise here does not appear with increasing distance from the outer wall. However, a strikingly flatter curve is found at the points concerned. Here, the curve for 180° is not shown, because the static pressure had probably already been affected by the transmission section to the fan located behind the chamber. The situation was different in series H, where the chamber sheet metal at the exit extended another 20 cm parallely to the motor axis. The total pressure curves present a somewhat different picture from those of the strong curvature (Series H, Fig. 13). The pressure drop is very slightly stronger; accordingly, the boundary layer does not remain constant but increases up to complete disappearance of the potential flow after about 15 mm. At the outer wall the boundary layer thickness increases with the angle significantly more rapidly than isthe case in Series F. Here, however, one must take into consideration, in addition tothe increased turbulence exchange, also the longer distances the particles must travel. The curves for the static pressures are much flatter than the corresponding ones for Series H. The total and static pressure curves for different average velocities show tolerable close affinity. Accordingly, an appreciable influence of the Reynolds number does not seem to appear at the velocities 12.7 to 19.3 m/sec used. Therefore the curves for a series of measurements were shown only for an average velocity of v_m = 18.4.

The ideal case of a friction-free flow in the curved chamber is that of a velocity inversely proportional to the radius: $v = k/r$. Here, k is a constant determined by the size of the chamber and the average velocity. In these investigations an 180° curved chamber was now attached to a straight entrance channel. The symmetrical velocity distribution which in the abstract exists in the straight channel seeks, just prior to entering the curved chamber, to conform to the flow pattern in the chamber, i.e., the hyperbolic distribution. This means that already in the straight channel

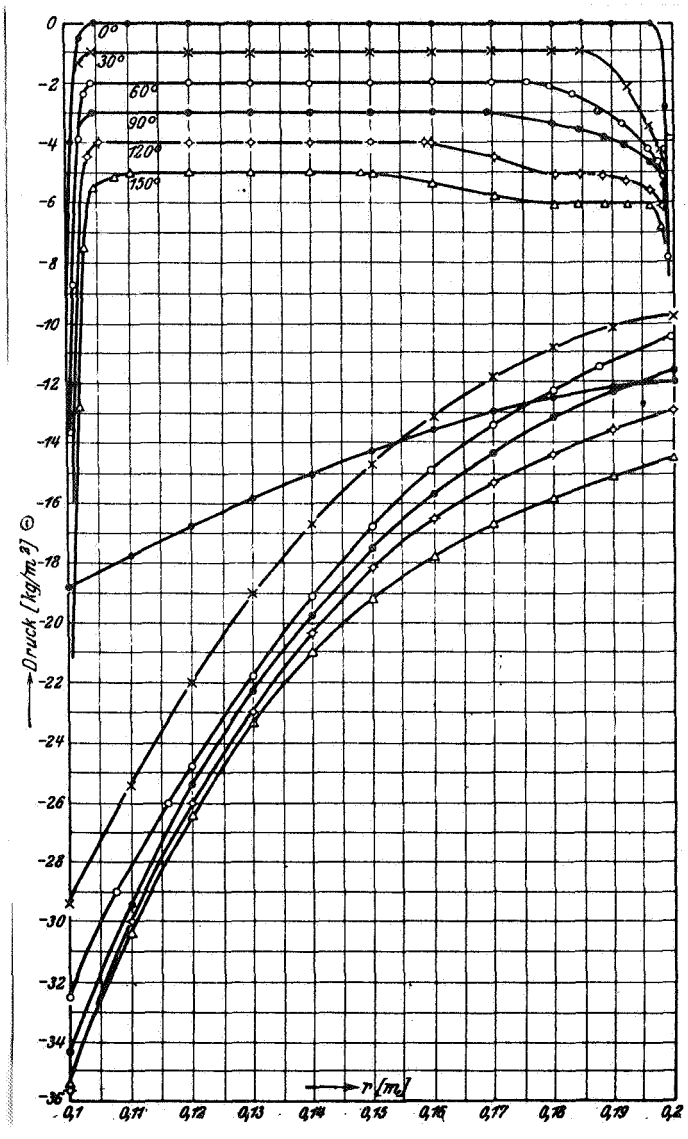

Fig. 12. Total pressure (upper) and statical pressure (lower) for experiment series F. (Strong curvature, without entrance channel.) v_m = 15.4 m/sec. Concerning the pressure scale, see Fig 11.

[Legend]: 1) pressure.

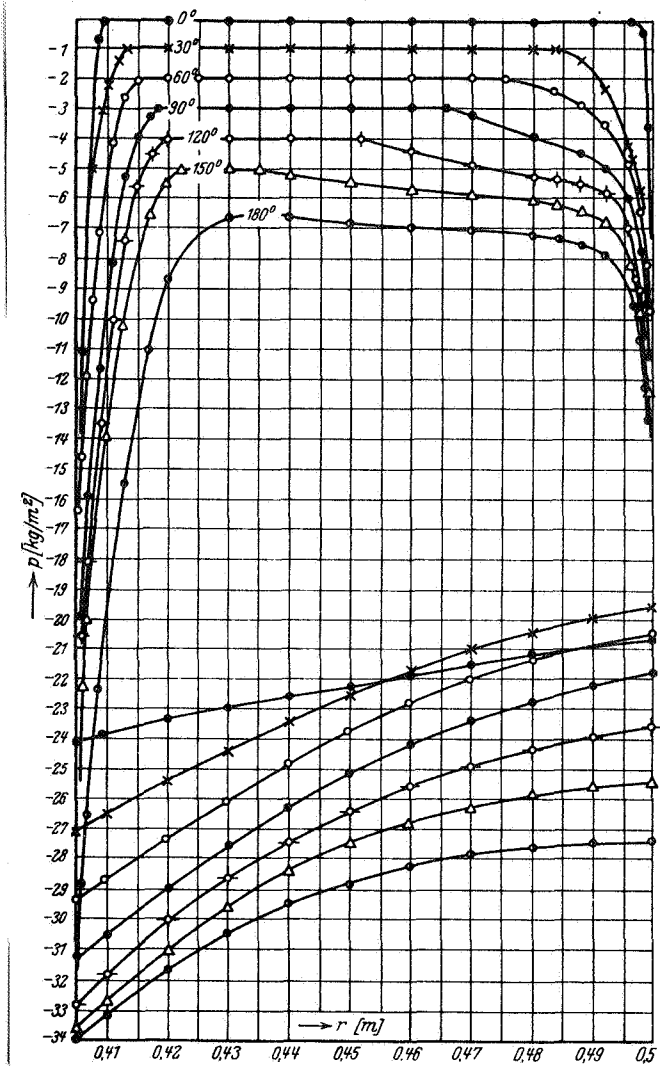

Fig. 13. Total pressure (upper) and statical pressure (lower) for experiment series H (weak curvature). v_m = 18.4 m/sec. Concerning the pressure scale, see Fig 11.

there exists a pressure increase or pressure reduction. On the outer side this pressure increase is considerably reinforced upon entrance into the curved chamber. If we now consider the velocities in a chamber with strong curvature and an entrance channel of one meter (Fig.14) and thus showing a boundary layer thickness of about 2.5 cm at each side at the

beginning of the chamber curve, traced over the radii and dependent upon the angle, we see that the approximation to the hyperbolic distribution is completed between 0° to 90°. The dashed curve [on the graph] always represents the ideal velocity distribution. In an arrangement without the entrance channel also, an asymmetrical velocity distribution obtains already at the entrance to the curvature (Fig 15), since the pressure rise or pressure drop already exercise their influence upon the flow. To be sure, there exists here an essential variation, namely that the boundary layers at first amount to only a few millimeters; therefore the thickening caused by the pressure rise does not in itself amount to much, and a spread-out potential flow thus exists between the boundary layers. The velocities were here determined simply by the static pressure, and a good approach to the ideal distribution of the potential flow may be expected. As shown in Fig. 15, a very good approximation is reached already at 30°. If the chamber wills are only weakly curved, a sharp transition of the not quite symmetrical distribution (Fig. 16, experiment series H) at the entrance to the curved chamber to a hyperbolic one is not present, because even the entire variation is not large enough. Boundary layer thicknesses increase at both sides. The initial pressure drop at the inner wall and the increase at the outer wall come to an end at approximately 60° (Figs 9 and 10), which is also shown by the changes in the velocity. Toward the end of the curved chamber the transition to symmetrical flow is noticeable. At 180° the profile again approaches that at 0°.

The radial velocities were calculated on the basis of the continuity conditions. It proved that in experiment series F (Fig 17) they could at the beginning of the curved chamber amount to approximately 10% of the average velocity. And here, of course, they are directed inward, i.e., negatively, if we designate the direction from the center outward as positive. A thin silk thread inserted into the flow also shows a deviation from the tangential direction. At larger angles the transverse velocities sink to lower values and toward the end of the curved chamber they once more approach larger positive values. The main flow seeks at the end of the chamber once more to approach a symmetrical distribution.

In the arrangement with weak curvature (experiment series H, Fig 18) the radial velocities w are very small, corresponding to the small changes in the velocity profile. At their highest value they did not even reach 1% of the average velocity (in Fig 18 the scale is ten times larger than

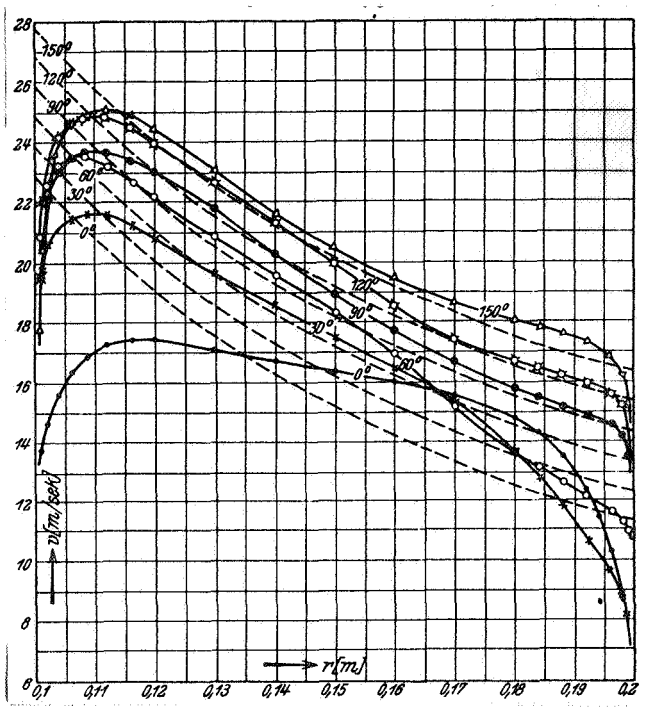

Fig. 14. Velocity profile for experiment series D (strong curvature, one-meter entrance channel). v_m = 15.5 m/sec. The scale for v is $\varphi = 0°$. The curves for the next angles are always displaced upward by 1 m/sec.

that in Fig 17.) In other respects, this profile shows almost the same characteristics of distribution over the cross section as the radial components present with greater curvature.

In order to show the affinity of the velocity profiles for various Reynolds numbers, the relationship of the velocities v to the mean velocity v_m for the three mean speeds use was drawn in Fig 19 for the 90° cross section of experiment series D. It is seen that the curves for various mean speeds used was drawn in Fig 19 for the 90° cross section of experiment series D. It is seen that the curves for various mean speeds agree tolerable well.

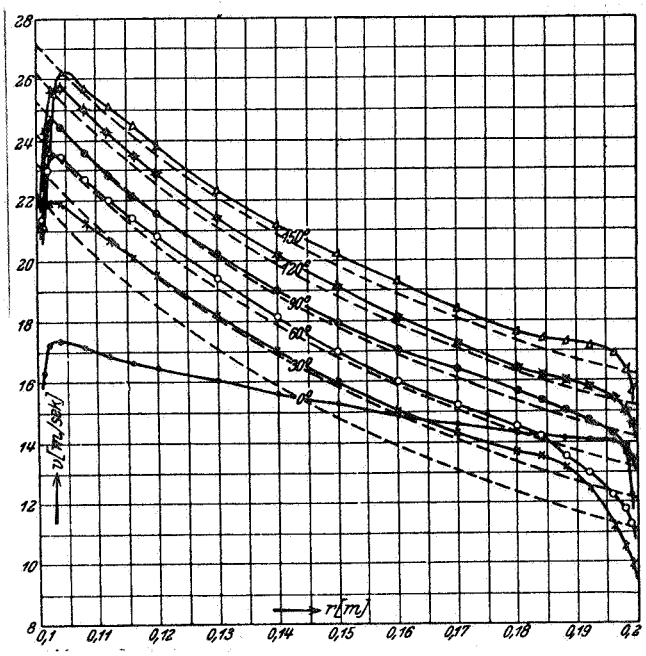

Fig. 15. Velcotiy profile for experiment series F (strong curvature, without entrance channel.) v_m = 15.4 m/sec. Concerning the velocity scale, see Fig. 14

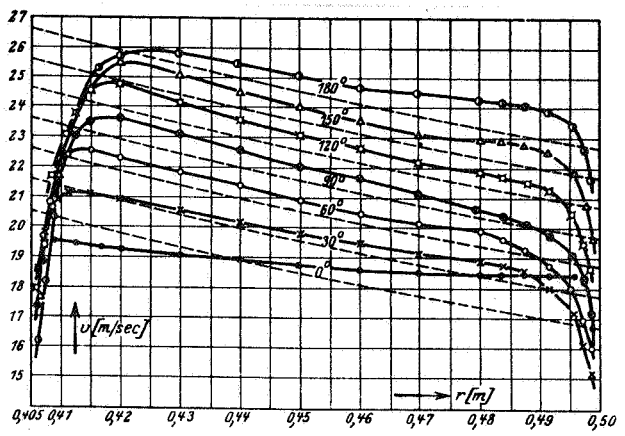

Fig. 16. Radial velocities for experiment series H (weak curvature). v_m = 18.4 m/sec. Concerning the velocityscale, see fig. 15.

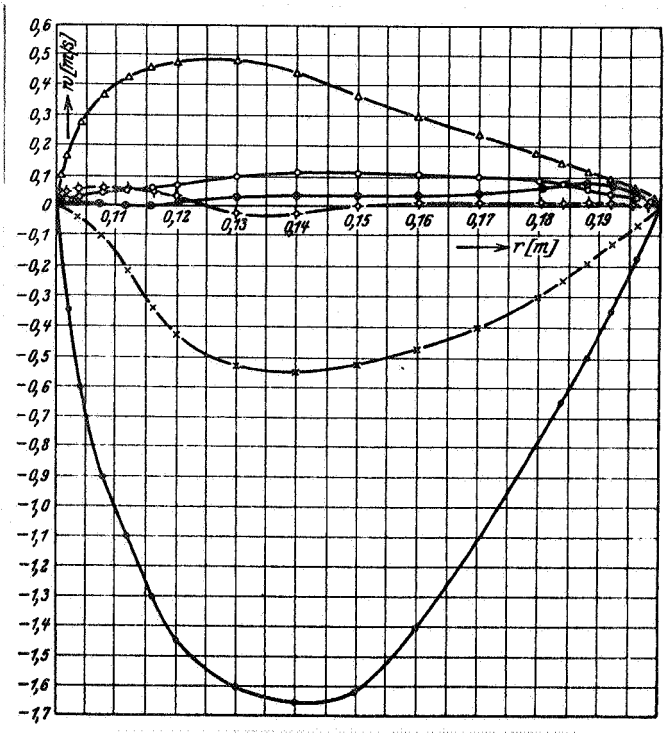

Fig. 17 Radial velocities for experiment series F (strong curvature, no entrance chamber.) v_m = 15.4 m/sec

II. Evaluation of the Experiments

1. Calculation of the Tangential Stresses

For calculation of the tangential stresses over a cross section, one takes a middle horizontal layer of thickness 1 and considers an element with the radii r and r + dr and angular aperture $d\varphi$ (Fig 20) and applies the theorem of momentum which states that the moment of the impulse appearing on the surface of a fluid in a limited space (emerging impulse negative) is in balance with the moment of the exterior force acting upon it.

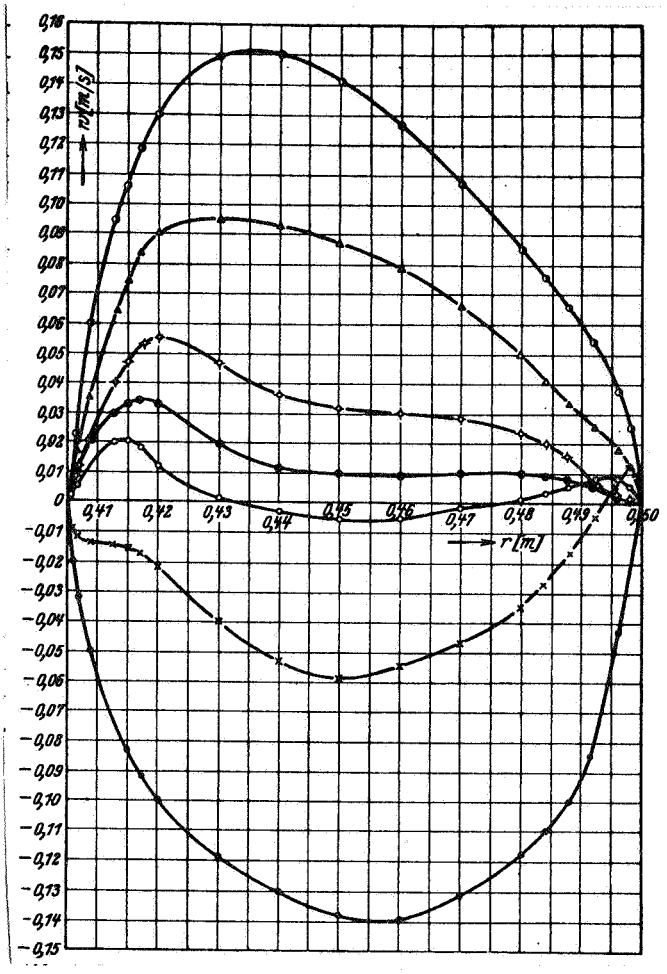

Fig. 18. Radial velocities for experiment series H (weak curvature.) v_m = 18.4 m/sec.

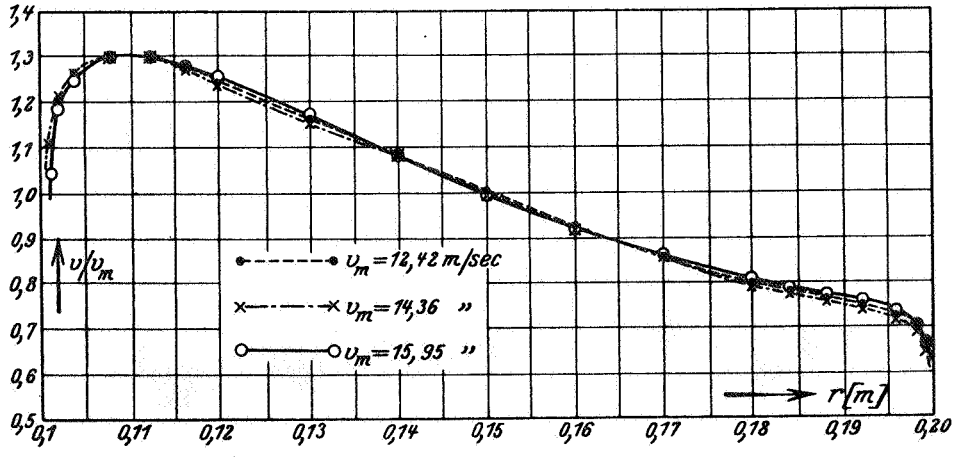

Fig. 19. Comparison of Velocity profiles at $\varphi = 90°$ for experiment series D for three different mean velocities.

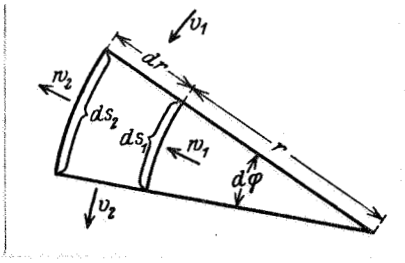

Fig. 20.

One obtains:

1. The impulse moment of the fluid flowing in the tangential direction

$$-\varrho r \frac{dv^2}{d\varphi} dr\, d\varphi,$$

2. The moment of the pressure

$$-r \frac{dp}{d\varphi} dr\, d\varphi,$$

3. The impulse moment of the fluid flowing in the tangential direction

$$-\varrho \frac{d(r^2 w v)}{dr} dr\, d\varphi,$$

4. The moment of the tangential stress

$$\frac{d(\tau r^2)}{dr} dr\, d\varphi.$$

These four moments must be in balance. This gives

$$\begin{aligned} \frac{d(\tau r^2)}{dr} &= r \frac{dp}{d\varphi} + r\varrho \frac{dv^2}{d\varphi} + \varrho \frac{d(r^2 w v)}{dr} \\ &= r\left(\frac{\varrho}{2} \frac{dv^2}{d\varphi} + \frac{dp}{d\varphi}\right) + r \frac{\varrho}{2} \frac{dv^2}{d\varphi} + \varrho w r^2 \frac{dv}{dr} + 2\varrho r w v + v r^2 \varrho \frac{dw}{dr}. \end{aligned} \tag{5}$$

The members $dp/d\varphi + \varrho dv^2/2d\varphi$ produce the differential quotient $dG/d\varphi$ of the total energy G [equation (2)] according to the angle. Thus we have

$$\frac{d(\tau r^2)}{dr} = r \frac{dG}{d\varphi} + r \frac{\varrho}{2} \frac{dv^2}{d\varphi} + \varrho w r \left(r \frac{dv}{dr} + v\right) + \varrho v r \left(w + r \frac{dw}{dr}\right). \tag{6}$$

The continuity gives the equation

$$\frac{d(rw)}{dr} + \frac{dv}{d\varphi} = 0 \quad \text{oder} \quad r\frac{dw}{dr} + w = -\frac{dv}{d\varphi}.$$

If equation (6) is now introduced, the equation is simplified to

$$\frac{d(\tau r^2)}{dr} = r\frac{dG}{d\varphi} + \varrho w r\left(v + r\frac{dv}{dr}\right). \qquad (7)$$

If one differentiates the equation G = p + $\varrho v^2/2$ according to r

$$\frac{dG}{dr} = \frac{dp}{dr} + \varrho v\frac{dv}{dr}$$

and writes according to (1)

$$\frac{dp}{dr} = \frac{\varrho v^2}{r} - \varrho v\frac{dw}{r\,d\varphi}$$

(centrifugal acceleration), one obtains

$$\frac{dG}{dr} = \frac{\varrho v^2}{r} - \varrho v\frac{dw}{r\,d\varphi} + \varrho v\frac{dv}{dr} = \frac{\varrho v}{r}\left(v + r\frac{dv}{dr}\right) - \frac{\varrho v}{r}\frac{dw}{d\varphi}$$

or

$$v + r\frac{dv}{dr} = \frac{r}{\varrho v}\frac{dG}{dr} + \frac{dw}{d\varphi}.$$

If one introduces this value into equation (7) one obtains

$$\frac{d(\tau v^2)}{dr} = r\frac{dG}{d\varphi} + r^2\frac{w}{v}\frac{dG}{dr} + \varrho w r\frac{dw}{d\varphi}. \qquad (8)$$

The integral between the limits r_i (radius of the inner wall) and r gives the final result:

$$\tau r^2 = \int_{r_i}^{r}\left(r\frac{dG}{d\varphi} + r^2\frac{w}{v}\frac{dG}{dr} + \varrho w r\frac{dw}{d\varphi}\right)dr$$

or

$$\tau = \left(\frac{r_i}{r}\right)^2\left[\tau_i + \frac{1}{r_i^2}\int_{r_i}^{r}\left(r\frac{dG}{d\varphi} + r^2\frac{w}{v}\frac{dG}{dr} + \varrho w r\frac{dw}{d\varphi}\right)dr\right]. \qquad (9)$$

The term $dw/d\varphi$ can be ignored in the evaluation since it is not very large. In this equation (9) for the tangential stress τ all values are given by experimental data, or can be determined from them.

The differential quotients $dG/d\varphi$ and dG/dr must be determined graphically. The tangential stress at the inner wall is determined on the basis of the tangential stress in the potential flow. This is

$$\tau = \mu\left(\frac{dv}{dr} - \frac{v}{r} + \frac{dw}{r\,d\varphi}\right),$$

which with v = k/r and w = 0 gives

$$\tau = -2\mu\frac{k}{r^2}$$

Compared to the tangential stresses in the friction layer this is so small that it can be assigned zero value; this produces

$$\tau_i = -\frac{1}{r_i^2}\int_{r_i}^{r_{Pot}}\left(r\frac{dG}{d\varphi} + r^2\frac{w}{v}\frac{dG}{dr}\right)dr. \qquad (10)$$

The wall tangential stress τ_i can be found also in another way, which may serve as a check. One considers an element of the horizontal section of depth 1, enclosed by the radii r_i and r_o and the lines of the basic angle; r_o is a radius at which the potential flow exists. Thus the deliminated element extends from the wall of the curved chamber through the boundary layer to the potential flow. If one now considers the changes in the impulse moments and the force moments, one obtains:

1. The moment of the impulse difference in the tangential direction

$$\int_{r_i}^{r_o} r\varrho v_1^2\,dr - \int_{r_i}^{r_o} r\varrho v_2^2\,dr,$$

2. The moment of the pressure difference

$$\int_{r_i}^{r_o} r p_1\,dr - \int_{r_i}^{r_o} r p_2\,dr,$$

3. The moment of the impulse transfer through the outer delimiting surfaces as a result of the radial velocity differences

$$-\varrho\int_{\varphi}^{\varphi+1} w_0 r_0^2 v_0\,d\varphi.$$

According to the impulse theorem one writes

$$\tau_i r_i^2 = \int_{r_i}^{r_0} \varrho r v_1^2 dr - \int_{r_i}^{r_0} \varrho r v_2^2 dr + \int_{r_i}^{r_0} r p_1 dr - \int_{r_i}^{r_0} r p_2 dr - \varrho \int_{\varphi}^{\varphi+1} w_0 r_0^2 v_0 d\varphi . \qquad (11)$$

Turning now from the differences to the differentials, with concentration of the terms

$$\int_{r_i}^{r_0} \varrho r v_1^2 dr + \int_{r_i}^{r_0} \varrho p_1 dr \quad \text{usw.},$$

one obtains

$$\tau_i r_i^2 = \int_{r_i}^{r_0} r \frac{dG}{d\varphi} dr + \varrho \int_{r_i}^{r_0} r v \frac{dv}{d\varphi} dr - \varrho w_0 v_0 r_0^2 . \qquad (12)$$

On the basis of the continuity, one can write

$$\varrho \int_{r_i}^{r_0} \frac{dv}{d\varphi} dr = \varrho w_0 r_0 .$$

Introduced into equation (12), this results in

$$\tau_i r_i^2 = \int_{r_i}^{r_0} r \frac{dG}{d\varphi} dr + \varrho \int_{r_i}^{r_0} \left(r v \frac{dv}{d\varphi} dr - \frac{dv}{d\varphi} r_0 v_0 \right) dr$$

$$\tau_i = \frac{1}{r_i^2} \int_{r_i}^{r_0} \left[r \frac{dG}{d\varphi} + \varrho \left(r v \frac{dv}{d\varphi} - r_0 v_0 \frac{dv}{d\varphi} \right) \right] dr . \qquad (13)$$

In this equation also, all values are determined through the experiments.

2. The Apparent Kinematic Viscosity and the Free Path of the Turbulent Exchange Movement

For a laminar flow along a straight wall the simple equation $\tau = \mu \cdot dv/dy$ applies; if for the viscosity one substitutes the kinematic viscosity $v = \mu/\varrho$, then $= \varrho v\, dv/dy$. If the flow becomes turbulent, the apparent kinematic viscosity ε takes the place of the kinematic viscosity v, but

here it should be taken into consideration that ε is not constant over the cross section. Just as ν is a measure of the impulse exchange among the individual molecules, which remains constant over the cross section, ε can be regarded as a measure of the impulse exchange of single trubulence complexes, and the exchange velocity of which does not remain constant over the cross section. The tangential stress is calculated from the impulse theorem [equation (9)]. On the other hand, the Boussinesq formula

$$\tau = \varrho\,\varepsilon\left(\frac{dv}{dr} - \frac{v}{r} + \frac{dw}{r\,d\varphi}\right). \tag{14}$$

applies to the curved chamber.

Equations (9) and (14) result in the following expression for the apparent kinetic viscosity

$$\varepsilon = \frac{\left(\frac{r_i}{r}\right)^2\left[\tau_i + \frac{1}{r_i^3}\int_{r_i}^{r}\left(r\frac{dG}{d\varphi} + r^2\frac{w}{v}\frac{dG}{dr}\right)dr\right]}{\varrho\left(\frac{dv}{dr} - \frac{v}{r} + \frac{dw}{r\,d\varphi}\right)}. \tag{15}$$

According to a formula by Prandtl, the apparent viscosity can now be further interpreted; it has the dimension [m^2/sec] and can be split into a velocity u and a length l. Here l indicates the mean stopping distance of a turbulence complex; this has the same meaning at the free path of the molecules in the kinetic category. The velocity u is then the mean transverse velocity at which the turbulence complexes pass through the surface of a layer from both sides. Prandtl showed that $\varepsilon = \mu l$ up to a proportionality factor included in the value of l. For the median transverse velocity u in a linear flow it is further assumed that the difference in velocity between two adjacent flows with velocities v + 2/2 and v 2/2 dv/dy dv/dy, between which impulse exchange occurs, is proportional (y = path vertical to direction of flow.)

Thus one writes

$$u = l\left|\frac{dv}{dy}\right|$$

and thereby, when here also the proportionality factor is included.

$$\varepsilon = l^2 \left| \frac{dv}{dy} \right| \quad \text{or} \quad l = \sqrt{\frac{\varepsilon}{\left| \frac{dv}{dy} \right|}}. \tag{16}$$

In the case of curved flow lines, a "natural" velocity drop is present already in the potential flow. For appropriate application of Prandtl's theorem one must therefore replace dv/dy by d/v - v/y.

$$l = \sqrt{\frac{\varepsilon}{\left| \frac{dv}{dr} - \frac{v}{r} \right|}}. \tag{17}$$

3. The Values Found for τ, ε and l

The tangential stresses τ calculated according to equation (9) are shown in Figs 21, 22, and 23. It is seen that tolerable smooth curves can be drawn through the separate values, and that only a few points fall outside the curves. The curves for 180° were left out because here the determination of the differential quotient dG/dφ was to unsure. Similarly the radial velocities for 180° must be extrapolated, so that here also, inaccuracies of some size might result. For the tangential stresses at 0° large errors might appear through inexact determination of the mentioned values.

The tangential stress curves run approximately as follows: From a certain positive value at the inner wall, the values fall off to close to zero in the potential flow. As soon as the outer boundary layer appears, the τ values very rapidly take on higher negative values and are then, gradually decreasing in value, transferred to the outer wall. In the case of strong curvatures, the curve in some cases rises again somewhat toward the outer wall; the tangential stress is thus once more reduced somewhat toward the outer wall. The tangential stress in the inner boundary layers of the curved chamber presents little that is noteworthy. Here, the boundary layer thicknesses changes only little, for the tangential stress curves run, according to pressure conditions, more or less steeply. A maximum directly on the wall is reached where the transition to asymmetrical flow is at an end. A significantly more interesting picture is presented by the tangential stress curves for the outer curved surface. Where the velocity distribution approaches the ideal (end of

the transition area) a pressure maximum lies at the outer wall. These points, according to the measurements, lie about in the area between 30° and 60°. According to the impulse theorem for tangential stress, a minimum at the outer wall and a maximum at the inner wall result here. If a very strong pressure rise should result at the outer wall, i.e., much velocity energy be transformed into pressure energy, the tangential stress would finally drop to zero, or even become negative. This means that at the outer wall the particles would no longer move forward, or would even wander backward. In these cases, eddies appear. Although in the investigated curved chambers no eddies appeared, an obvious drop in the tangential stress toward the wall was found in experiment series D and F, which is to be regarded as the preliminary stage to the formation of eddies.

For determination of the apparent kinematic viscosity ε one must divide the value for τ [equation (9)] by the value

$$\varrho\left(\frac{dv}{dr}-\frac{v}{r}+\frac{dw}{r\,d\varphi}\right)$$

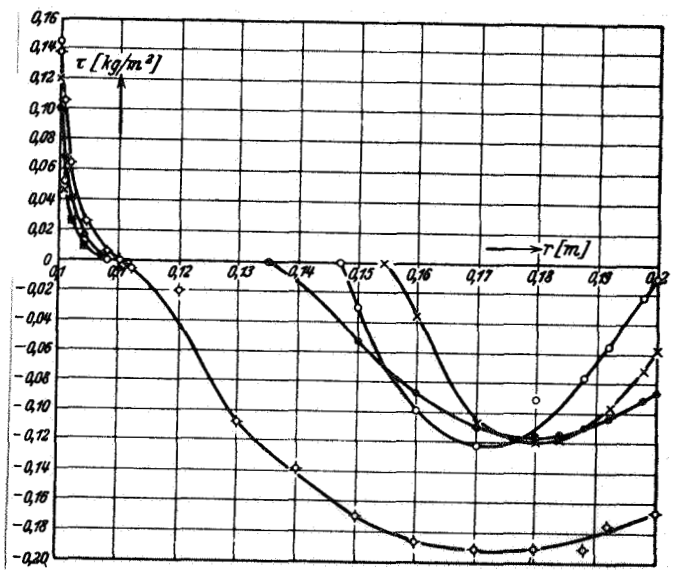

Fig. 21. Distribution of tangential stresses in experiment series D (Strong curvature, one-meter entrance chamber. v_m = 15.95 m/sec.

The term $dw/rd\varphi$ can be eliminated, since at the most it amounts to only a few percent of the other two terms, and since the uncertainty of the other two terms is usually considerably greater, particularly if it is a case of a graphically found differential quotient.

Consideration of the obtained curves (Figs 24, 25) shows that the apparent kinematic viscosities in the inner boundary layer are, in contrast to those in the outer boundary layer, very small. This means that the inner boundary layer is considerably more stable than the outer one. At the outer curved surface the value ε at the transition of the potential flow in the boundary layer rises very rapidly, increases with the growing angle, and at 150° reaches 500 times the value of the kinematic viscosity.

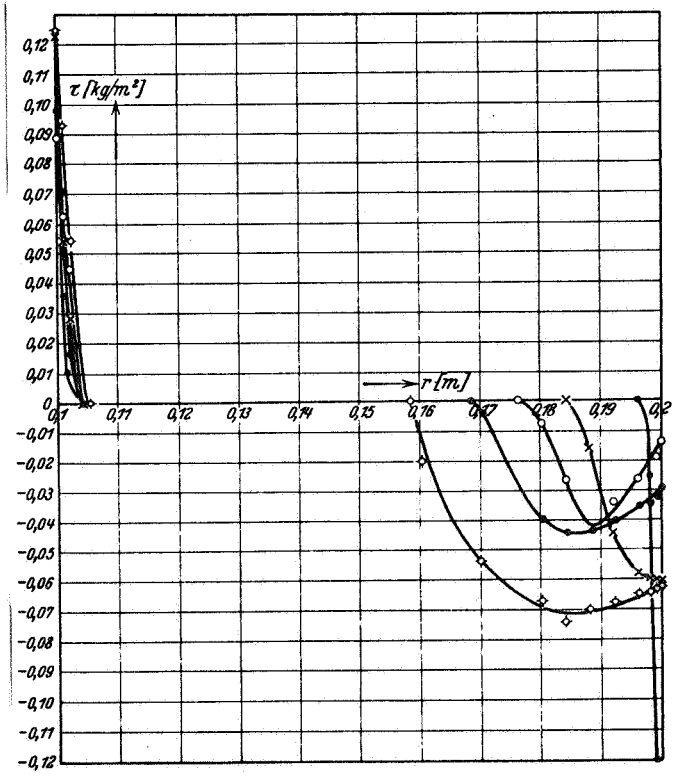

Fig. 22. Distribution of tangential stresses in experiment series F (strong curvature, without entrance chamber.) v_m = 15.4 m/sec

In the work by Doench similar increases were found in the apparent viscosity. For the purpose of determining to what extent the pressure rise in the first part of the curved chamber in our experiments has an effect, the ratio of the pressure rise in a path at the entrance to the chamber equal in length to the thickness of the boundary layer to the dynamic pressure of the unaffected velocity $\ell/2$ 2/0 may be selected as a scale for comparison. In the work by Doench the value of about .02 resulted for this with a channel of .81° widening. In experiment series H it is in the area of φ= 0° to

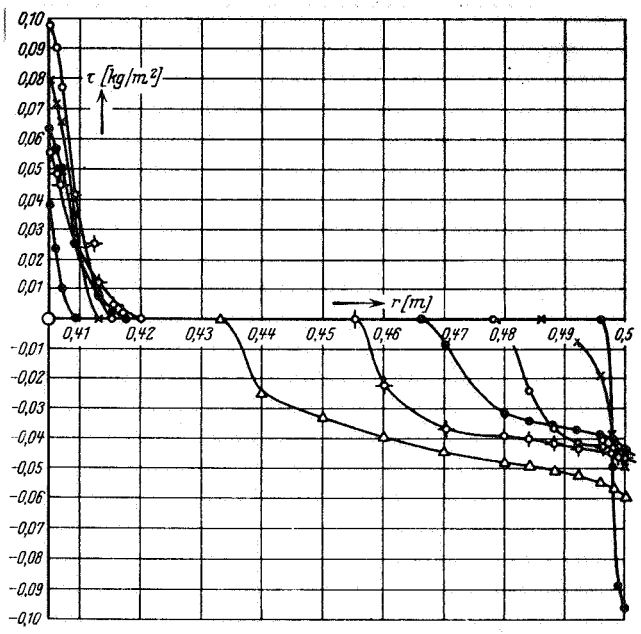

Fig. 23. Distribution of tangential stresses in experiment series H (weak curvature.) v_m = 18.4 m/sec

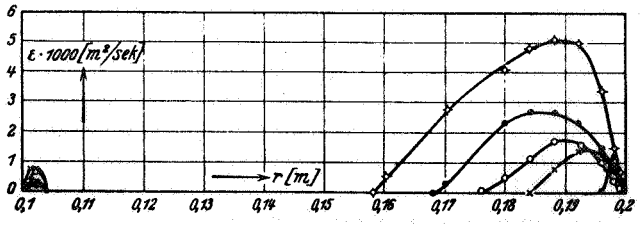

Fig. 24. Apparent kinematic viscosity ε in experiment series F (Strong curvature, without entrance channel.) v_m = 15.4 m/sec. (Curve characteristics as in Figs 11 to 13.)

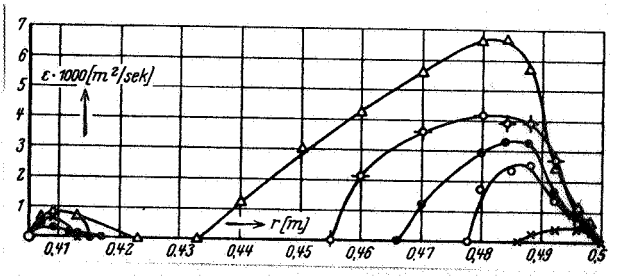

Fig. 25. Apparent kinematic viscosity ε in experiment series H (weak curvature.) v_m = 18.4 m/sec. (Curve characteristics as in Figs 11 to 13.)

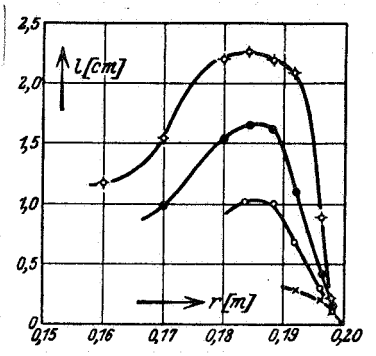

Fig. 26. Exchange paths in experiment series F

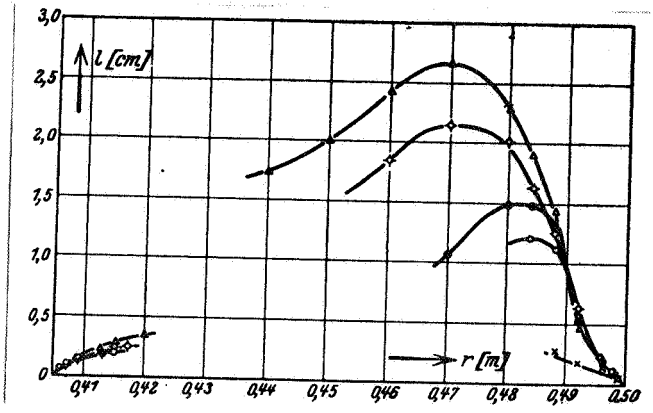

Fig. 27. Exchange paths in experiment series H

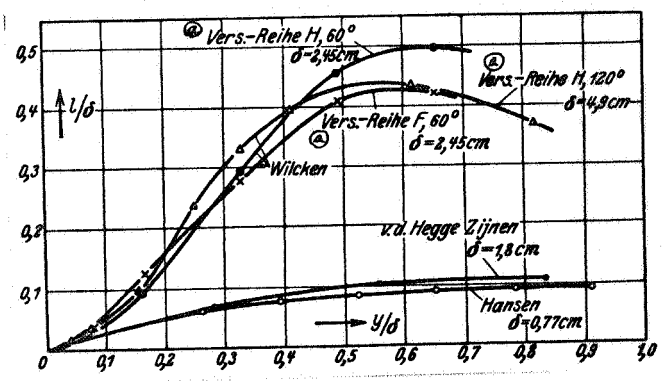

Fig. 28. Comparison of exchange paths for straight and curved surfaces

[Legend]: a) Experiment series.

φ = 30° about .0055, or only one fourth of that found by Doench. It can therefore very well be assumed that the relatively small pressure rise is of no decisive importance; moreover in experiment series H, at the angle of $\varphi > 30°$ no influence of the pressure rise is apparent. Thus one is justified in ascribing the development of ε, and thereby the development of the boundary layer, mainly to the effect of the curvature. This also makes it likely that in experiment series H, as well, in which the effect of the pressure rise cannot be separated from that of curvature, the changes found in the tangential stresses and the apparent viscosity must be ascribed to the effect of the curvature.

When at the beginning of the curved chamber a thicker boundary layer is present, as in experiment series D, the situation is different. The pressure rise at the outer wall will here certainly exert a greater influence, for here the total pressure curves (Fig 11), which also give the boundary layer thickness, show that from 0° to 30° the boundary layer thickness increases much more rapidly than is the case with weaker or stronger curvatures with initially thinner boundary layers. The influence of the pressure rise cannot very well be separated from that of the curvature.

Figs. 26 and 27 show according to equation (17) the curves of l values for experiment series F and H. At 150°. the l values reach the maximum value of 2.6 cm. In experiment series F the curves at the outer wall rise somewhat more steeply than the corresponding curves for the H series. In other respects they are similar. Within the potential flow

the values are undetermined, since here the denominator of the root [dv/dr - v/r] becomes zero. In the inner boundary layer the free paths reach no high values. In experiment series F the magnitude of l in the inner boundary layer is even smaller than in Series H. Thus the turbulence at the inner side is reduced with reduced curvature.

Finally, l curves at the outer wall at 60° and 120° for experiment series H and F were compared to l curves at a straight wall (Fig 28.) Values for the outer wall were calculated from velocity and boundary layer data in a work by van der Hegge Zijnen[8] and a work by Hansen[9]. The ratio of the distance of the wall y to the boundary layer thickness δ was taken as the abscissa and the ratio l/δ as the ordinate. The border layer thickness δ is here the distance from the wall to the potential flow. The curves for the curves chamber show a considerable deviation from those of the straight wall.

Summary

These experiments were undertaken for the purpose of determining whether events in turbulent boundary layers were affected by a curvature in the surface. Of the experiment series carried out, series H and F, in which the inner and outer curved surfaces were separated by a layer of potential flow, were in the main evaluated, along with, in part, series D. A theoretical consideration of impulses produced formulas for calculation of tangential stress τ and thereby the exchange value of ε of the impulse (the apparent kinematic viscosity), as well as the free path l of the turbulent exchange moment connected with it. A comparison of the l curves with those of a straight path produced much higher values than those for the straight plate.

Although the obtained results were made somewhat obscure by disturbing secondary influences, caused in particular by the pressure conditions obtaining at the entrance and exit to the curved chamber, they may in the main be attributed to the curvatures. The results reported are in many respects still imcomplete, but they nevertheless show that boundary layer events at curved surfaces should be ascribed more importance than has generally been the case up to the present, in that at concave surfaces the turbulence is very greatly increased, while at convex surfaces it is reduced.

BIBLIOGRAPHY

1. Goettingen Dissertation. Authors: Prof. Dr. A. Betz and Prof. Dr. L. Prandtl.

2. L. Prandtl: "On Flow Movement at Very Slight Friction," Proceedings at the International Mathematics Congress, Heidelberg 1904, (Reprinted in Prandlt-Betz: "Four Treatises on Hydrodynamics and Aerodynamics," Berlin 1927.

3. Th. v. Karman, Journal of Applied Mathematics and Mechanics (Zs f. ang. Math. u. Mech). I, 1921, p 233; van der Hegge Zijnen: "Measurements in the Boundary Layer along a Plane Surface; Thesis, Delft, 1924.

4. Doench, "Divergent and Convergent Turbulent Flow at Small Opening Angles," Reports on Research Work published by the VDI, No 282, 1926.

5. W. Fritsch, Journal of Applied Mathematics and Mechanics, 8, 1928, p 199.

6. Carried out at the suggestion of Prof. Dr. Betz, of the Kaiser Wilhelm Institute for Flow Research.

7. W. v. Cordier, "Flow Investigations in a Curved Tube." Dissertation, Berlin, 1910; Jaeger, Turbine Journal (Zs f. d. ges. Turbinenwesen), 1909, p 341; Isaachsen, Zs V. d. i., I, 1911, p 215; Lell, "Contribution to the Knowledge of Secondary Flows in Curved Chambers," Dissertation, Darmstadt, 1913.

8. See 3 above.

9. Hansen, Journal of Applied Mathematics and Mechanics, 8 1928, p 185.

Kaiser Wilhelm Institute for Flow Research, Goettingen

(Received 24 March 1930.)